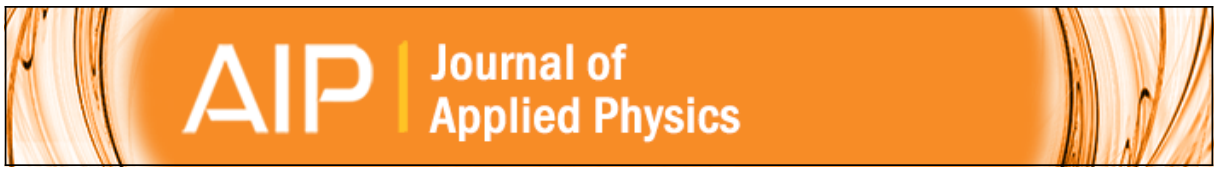

Ultrafast dynamics of hot electrons and phonons in chemical vapor deposited graphene

Kuan-Chun Lin, Ming-Yang Li, L. J. Li, D. C. Ling, C. C. Chi, and Jeng-Chung Chen

Citation: Journal of Applied Physics **113**, 133511 (2013); doi: 10.1063/1.4799377

View online: http://dx.doi.org/10.1063/1.4799377

View Table of Contents: http://scitation.aip.org/content/aip/journal/jap/113/13?ver=pdfcov

Published by the AIP Publishing

Ultrafast dynamics of hot electrons and phonons in chemical vapor deposited graphene

Kuan-Chun Lin,[1] Ming-Yang Li,[1] L. J. Li,[1,2] D. C. Ling,[3] C. C. Chi,[1,4] and Jeng-Chung Chen[1,4]
[1]*Department of Physics, National Tsing-Hua University, Hsinchu 30013, Taiwan*
[2]*Institute of Atomic and Molecular Sciences, Academia Sinica, Taipei 11529, Taiwan*
[3]*Department of Physics, Tamkang University, Tamsui Dist., New Taipei City 25137, Taiwan*
[4]*Frontier Research Center on Fundamental and Applied Sciences of Matters, National Tsing Hua University, Hsinchu 30013, Taiwan*

(Received 9 January 2013; accepted 19 March 2013; published online 4 April 2013)

The relaxation dynamics of photoexcited carriers in a chemical vapor deposited graphene transferred on quartz substrate has been investigated by using ultrafast optical-pump terahertz (THz)-probe spectroscopy. Terahertz transmission through graphene sample is reduced by optical pumping. The change of transmission decays exponentially after the optical pulse. We find the relaxation time is insensitive to the substrate temperature from 10 K to 300 K but increases sublinearly with pump fluence. We model the relaxation process involving electron-phonon coupling together with a set of rate equations to describe the transient responses of quasi-particles and optical phonons. The increases of the extracted carrier temperature and the measured relaxation time with pump fluence are associated with the fact that high pump fluence significantly increases the carrier temperature and broadens the carrier distribution. As a result, it leads to the reduction of optical phonon emission efficiency and the decrease of cooling rate as well. © *2013 American Institute of Physics*. [http://dx.doi.org/10.1063/1.4799377]

I. INTRODUCTION

Graphene is a single atomic layer of carbon atoms forming a two-dimensional honeycomb crystal lattice structure with a zero bandgap and a linear dispersion relation for both electrons and holes.[1] The unique electrical and optical properties and the high mobility of carriers in graphene make it a promising material for high speed electronics, photonics, and optoelectronic devices, such as field-effect transistors, broadband optic sensors, and THz oscillators.[2–6] Recent advances in large-area, single-layer graphene fabrication have further demonstrated the potential to commercialize graphene-based devices.[7–9] To date, chemical vapor deposition (CVD), owing to the advantages of the production of high quality, large-scale, uniform single layer graphene and the capability to transfer graphene onto various substrates at low cost, has become the most practical growth technique of graphene for device applications.[10]

The linear electronic dispersion across the charge-neutral point implies that any photon energy can produce an electron-hole pair, which makes graphene ideal for a broadband optical sensor. The speed of such optoelectronic would critically depend on the scattering and relaxation mechanism in electron-hole dynamics. It is generally believed that both intraband and interband carrier-carrier relaxation are rather efficient. Earlier studies by time-resolved experiments reveal that the photoexcited carriers can be rapidly thermalized to a quasi-equilibrium Fermi distribution at an effective temperature T_e after tens of femtoseconds.[11] In subsequent picosecond duration, hot carriers dissipate energy and their number density reduces via intravalley and intervalley phonon scattering. As the excitation intensity is large, a significant population of nonequilibrium optical phonons can be generated. Eventually, the generated phonons dissipate through the cooling of graphene phonons. It is generally believed the main bottleneck of relaxation is the efficiency of energy exchange between excited electrons/holes and optical phonons.[12]

Despite numerous studies on the ultrafast carrier relaxation and recombination dynamics in graphene,[13–18] the nature of the interplay between hot electrons and phonons in graphene remains inconclusive. The reasons are summarized in the following. First, the relaxation process involved with the interaction of hot electrons and phonons has not been discreetly considered in the analysis of experimental data.[15,17] Second, epitaxial graphene grown on SiC and CVD graphene grown on nickel are mixed with mono- and multi-layer graphene sheets. Moreover, graphene on SiC is strongly coupled to the substrate.[16,17] It makes the ultrafast intrinsic carrier dynamics of monolayer graphene not be distinctly resolved. Third, typical optical pump-probe spectroscopy only samples the high energy tail of carrier distribution. It cannot provide suitable energy band to investigate the comprehensive relaxation dynamics in graphene.

In this work, we report the studies of ultrafast carrier dynamics of CVD-grown monolayer graphene on quartz substrate by time-resolved optical-pump THz-probe spectroscopy. Experimental findings show that the terahertz (THz) probe is mostly influenced by free carriers involved in the intraband scattering. Our aim is to elucidate the role of phonon generation and dissipation and carrier temperature in electron-hole generation and recombination rate. Our results show that the relaxation time is insensitive to the bath temperatures; in

contrast, it increases with the increase of pump fluence. At higher pump fluence, the electron-hole recombination rate can be suppressed by the substantial broadening of carrier distributions due to high carrier temperatures, which slows down the recombination rate of photoexcited carriers. We adopt a theoretical model, including electron-phonon coupling to have a comprehensive understanding of our experimental data.

II. EXPERIMENTAL SETUP

The CVD graphene studied was grown by decomposition of methane on copper foils. The detailed fabrication parameters and the transfer procedure have been reported in our previous work.[19] Micro-Raman spectroscopy with 473 nm laser of a spot size $\sim 1\,\mu m^2$ was carried out to characterize the quality of transferred graphene. Figure 1(a) shows a representative Raman spectrum of CVD graphene. The full width half maximum (FWHM) of 2D peak ($\sim 2700\,cm^{-1}$) is about $33\,cm^{-1}$ with a single Lorentzian profile shape. A low intensity of disorder-induced D peak is observed at $\sim 1350\,cm^{-1}$. The inset of Fig. 1(a) shows spatial Raman map of the intensity ratio of 2D to G peaks (I_{2D}/I_G) with 90% of the area $I_{2D}/I_G \geq 2$, indicating high uniformity of monolayer graphene on quartz.[20] Our CVD graphene has been found to be highly hole-doped. At room temperature, Van der Pauw measurements of the transferred graphene reveal a hole carrier density $P \cong 1.9 \times 10^{12}\,cm^{-2}$ with mobility 1030 cm^2/Vs for sample S1 and $P \cong 1.5 \times 10612\,cm^{-2}$ with mobility 1490 cm^2/Vs for sample S2.

Ultrafast laser of pulse width $\cong 130$ fs from a 1 kHz Ti: sapphire regenerative amplifier with a center wavelength of 800 nm (1.55 eV) was used to simultaneously excite the samples and to yield THz radiation. THz pulses were generated by optical rectification with proper pulse front excitation in Zinc Telluride (ZnTe) crystal, then collimated and focused onto the samples with a pair of 90° off-axis parabolic mirrors with beam diameter of ~ 5 mm, which is much smaller than the sample size $\sim 10 \times 15\ mm^2$. The transmitted THz pulse was received by another ZnTe electro-optic sampling crystals for detection.[21] Typical area of CVD graphene are much larger than optical pump pulse beam size of $3.2 \times 3.2\ mm^2$. It, therefore, makes THz measurements easy to perform.

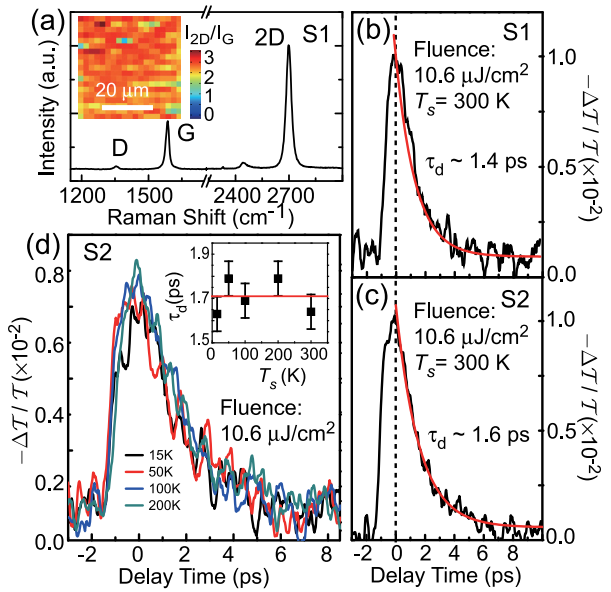

FIG. 1. (a) Representative Raman spectrum of CVD graphene transferred on quartz. Inset: Raman map of I_{2D}/I_G over a $40 \times 40\ \mu m^2$ area. Measured differential THz transmission $-\Delta\mathcal{T}/\mathcal{T}$ as a function of probe delay time for (b) sample S1 and (c) sample S2. The solid curves are fitted to the data using an exponential function with a relaxation time τ_d. The dashed line indicates the incident time of probe pulses. (d) Measured $-\Delta\mathcal{T}/\mathcal{T}$ transients of S2 at different substrate temperatures T_s. Inset: the extracted τ_d as a function of T_s.

III. EXPERIMENTAL RESULTS

Figures 1(b) and 1(c) show the pump-induced differential transmission (PIDT) of THz pulse, $-\Delta\mathcal{T}/\mathcal{T}$, through the CVD-grown monolayer graphene as a function of the probe delay time with a low pump fluence of $10.6\,\mu J/cm^2$ at room temperature for S1 and S2, respectively. The shape of terahertz pulse does not change through the graphene sample, so we only characterize the amplitude of THz pulse transmission. Here, $-\Delta\mathcal{T}/\mathcal{T}$ is the pump-induced change of transmission $-\Delta\mathcal{T}$ normalized to the transmission $\mathcal{T}$ without pump excitation. The negative sign is chosen so that $-\Delta\mathcal{T}/\mathcal{T}$ is a positive pulse with decay tail. Immediately after pump pulse excitation, PIDT is first rapidly increased in about hundreds of femtoseconds and followed by a slow decrease to a time scale of picosecond. The initial rapid increases represent the fast thermalization and thermal equilibrium by the carrier-carrier scattering with increasing the conductivity of graphene. The slow decrease of transmission is due to the gradually decreases of conductivity resulting from the electron-hole recombination. The evolution of signal peaks after ~ 100 fs can be phenomenologically fitted by an exponential decay with a time constant τ_d, i.e., $-\Delta\mathcal{T}/\mathcal{T} \propto \exp(-t/\tau_d)$, as shown in red curves. The extracted τ_d is about 1.4 ps and 1.6 ps for samples S1 and S2, respectively.

The THz-probe transmission is affected only by the change in the intraband absorption caused by the pump pulse. The transmission $\mathcal{T}$ of THz pulse through graphene and quartz substrate layer, normalized to the transmission through the substrate, can be described by[22]

$$\mathcal{T} = 1 \Big/ \left| 1 + \frac{Z_0 \sigma(\omega)}{n_s + 1} \right|, \quad (1)$$

where σ refers to the optical sheet conductivity of graphene, Z_0 is the vacuum impedance, and $n_s = 1.95$ is the refractive index of quartz substrate.[23] It is well established that the THz pulse absorption in graphene with near-infrared laser pumping is dominated by the intraband conductivity $\sigma(\omega)$,[22,24] which can be given by

$$\sigma(\omega) = i\frac{e^2/\pi\hbar^2}{\omega + i/\tau}\int_0^\infty [f(E-\mu_c, T_e) + f(E+\mu_v, T_e)]dE, \quad (2)$$

where τ is the momentum relaxation time, and μ_c and μ_v are the chemical potential for conduction band and valence band electrons with carrier temperature T_e, respectively. The zero energy point is defined to be at the Dirac point. The shorter τ_d of S1 with lower sheet conductivity and mobility

measured in the transport imply that impurity scattering plays an important role in the relaxation process. Since the absorption is directly related to the carrier occupations near μ_c and μ_v, in principle $\mathcal{T}$ is sensitive to carrier temperature. Figure 1(d) shows PIDT transients measured at different substrate temperatures T_s. Nevertheless, the measured transient exhibits an exponentially decaying with relaxation time τ_d insensitive to T_s as displayed in Fig. 1(d), in contrast to previous studies of epitaxial graphene on SiC.[16] We will discuss the differences with our model calculations in a later section.

To clarify the role of pump fluence in relaxation dynamics, PIDT transients measured at different pump fluences ($\mathcal{F}$) from 10.6 μJ/cm^2 to 89.1 μJ/cm^2 at T_s = 10 K are displayed in Figs. 2(a)–2(f). It is clear that PIDT immediately after photoexcitation apparently increases with $\mathcal{F}$. Meanwhile, the recovery tail of PIDT rises up with $\mathcal{F}$, suggesting longer relaxation time for stronger excitation. Extracted value of τ_d sublinearly increases with $\mathcal{F}$, as shown in Fig. 3. Increasing $\mathcal{F}$ causes τ_d to increase from ~1.35 ps at 10.6 μJ/cm^2 to ~2.18 ps at 89.1 μJ/cm^2. The photoexcited carrier density is estimated to increase from 7.2×10^{11} cm^{-2} at 10.6 μJ/cm^2 to 6.1×10^{12} cm^{-2} at 89.1 μJ/cm^2, which is comparable with the intrinsic doped carrier density at room temperature. Therefore, it is reasonable to assume that the carrier temperature increases significantly with pump fluence, accompanied with the generations of significant optical phonons.

IV. THEORETICAL MODEL AND DISCUSSION

The observations of longer τ_d associated with higher pump fluence provide compelling evidence that the coupling

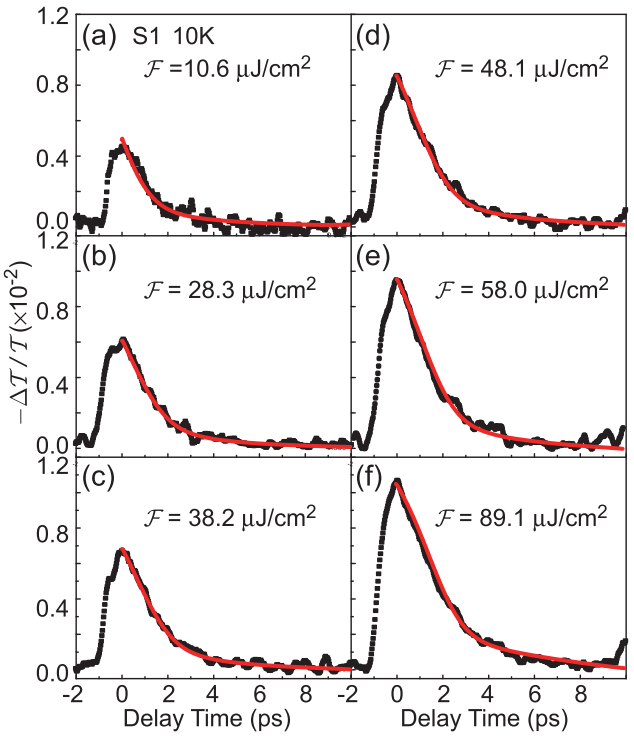

FIG. 2. Measured differential transmissions through graphene as a function of the probe delay at several different pump fluences ($\mathcal{F}$) (a) 10.6 μJ/cm^2 to (f) 89.1 μJ/cm^2. The substrate temperature was kept at 10 K. The red solid curves are the best-fit theoretical curves.

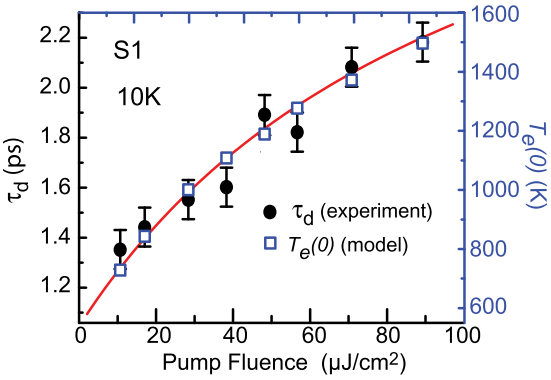

FIG. 3. The relaxation time τ_d and electronic temperature $T_e(0)$ are plotted as a function of pump fluence. $T_e(0)$ is referred to the carrier temperature right after the pump pulse excitations, i.e., the delay time ~0. τ_d (solid circle) is extracted from the exponential fit to Fig. 2. $T_e(0)$ (open square) is obtained by the model fit. The solid curve through $T_e(0)$ is a plot guided by eyes.

between hot electrons and optical phonons must be taken into account to elucidate the relaxation dynamics. A theoretical calculation of relaxation rate concerned electron-phonon scattering in graphene has been recently investigated by Rana *et al.*[12] They suggested that electron-hole recombination and generation rates become insensitive to carrier temperature up to 300 K at high carrier density limit (~10^{12} cm^{-2}). To reconcile with our findings, the carrier temperatures of samples studied seems to be much higher than 300 K. It has been shown that interband electron-phonon scattering are mainly attributed to two optical phonon modes: E_{2g}-mode near the zone center (Γ-point) and A_1'-mode at the zone edge (K-, K'-point).[12,18] Both transverse and the longitudinal optical phonon of E_{2g}-modes contribute to intravalley interband carrier scattering, while only transverse optical phonon of A_1'-mode contributes to intervalley interband scattering. To consider both intravalley and intervalley optical phonon scattering in relaxation dynamics, we adopt a model proposed earlier,[12,18] and incorporate a single carrier temperature and two chemical potentials (one for conduction band and the other for valence band) to characterize the nonequilibrium quasi-particles. Figure 4 shows a schematic diagram to illustrate a relaxation scenario involving interband phonon scattering. After reaching quasi-equilibrium, the photoexcited electron-hole pairs recombine via emitting optical phonons with energy $\hbar\omega_\Gamma$ and $\hbar\omega_K$ for the E_{2g} and A_1' phonons, respectively; thus lowering T_e and

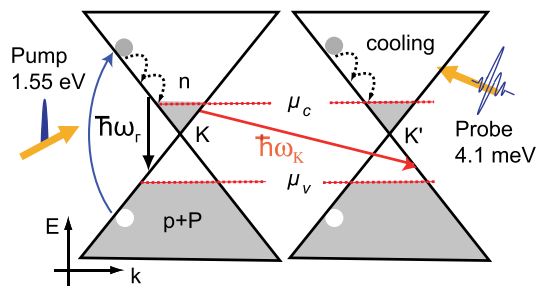

FIG. 4. A schematic diagram to illustrate relaxation processes of photoexcited carriers involving interband phonon scattering.[12]

photoexcited carrier density. The net recombination rate due to interband phonon scattering can be expressed as

$$R_q = \frac{9}{2}\frac{(\partial b/\partial t)^2}{\pi\rho\omega_q(\hbar v)^4}\int_0^{\hbar\omega_q} E(\hbar\omega_q - E)f(E-\mu_c,T_e) \times f(\hbar\omega_q - E + \mu_v,T_e)(n_q+1) - E(\hbar\omega_q - E)[1-f(E-\mu_c,T_e)] \times [1-f(\hbar\omega_q - E + \mu_v,T_e)]n_q\,dE, \quad (3)$$

where $q = \Gamma$ or K denotes the phonon mode at Γ- or K-points, respectively. n_Γ represents the phonon occupation numbers of E_{2g}-mode, while n_K for A_1'-mode. R_Γ and R_K are the net recombination rates for intravalley and intervalley interband electron scattering, respectively. The optical phonon energy are $\hbar\omega_\Gamma = 196\,\text{meV}$ and $\hbar\omega_K = 161.2\,\text{meV}$. $\partial t/\partial b \sim 53\,\text{eV/nm}$.[12] ρ is the density of graphene and equals to $\sim 7.6\,\text{kg/m}^2$. v_f is the Fermi velocity and equals to 10^6 m/s. $f(E-\mu,T_e) = 1/(e^{E-\mu/kT_e}+1)$ is the Fermi-Dirac distribution function for conduction and valence bands with carrier temperature T_e, assumed to be the same for both electron and hole.[25] The integrand in Eq. (3) includes the products of initial and final density states, and the probabilities of a phonon emission and absorption corresponding to the energy distribution of the electron-phonon scattering events. The THz response is mostly determined by the carrier densities; thus, we only consider the relaxation processes with reduced carrier densities, namely recombination events. For this reason, we limit integration range in Eq. (3) from zero to $\hbar\omega_q$.

The transient cooling process, depending on the interplay of the intrinsic doped carrier density (hole density P in our case), the photoexcited carrier density (electron n and hole p), average phonon occupation numbers (n_Γ and n_K), and the net recombination rate R_Γ and R_K, can be described by a set of coupled rate equations

$$\frac{dT_e}{dt} = -\frac{R_\Gamma\hbar\omega_\Gamma + R_K\hbar\omega_K}{C_e}, \quad (4)$$

$$\frac{dn_\Gamma}{dt} = \frac{R_\Gamma}{M_\Gamma} - \frac{n_\Gamma - n_\Gamma^0}{\tau_{op}}, \quad (5)$$

$$\frac{dn_K}{dt} = \frac{R_K}{M_K} - \frac{n_K - n_K^0}{\tau_{op}}. \quad (6)$$

Here, C_e is the carrier heat capacity, n_Γ^0 and n_K^0 are the phonon numbers in equilibrium, and τ_{op} is averaged life time of optical phonons. $M_\Gamma(M_K)$, the numbers of phonon modes per unit area at $\Gamma(K)$-points, is evaluated by integrating the wave vector of phonon from zero to ω_Γ/v_f (ω_K/v_f) (Ref. 26) to be consistent with Eq. (3). It follows that $M_\Gamma = 2/4\pi(\omega_\Gamma/v_f)^2$ and $M_K = 2/4\pi(\omega_K/v_f)^2$. The photoexcited carrier density and the chemical potential can be expressed as $n = 2/\pi(\hbar v_f)^2\int_0^\infty f(E-\mu_c,T_e)EdE$, and $p+P = 2/\pi(\hbar v_f)^2\int_0^\infty f(E+\mu_v),T_e)EdE$. In this approach, T_e and τ_{op} are the two fitting parameters.

The red solid curves shown in Fig. 2 are the theoretical fits. The value of carrier temperature extracted at the delay time near zero, $T_e(0)$, as a function of pump fluence $\mathcal{F}$ is plotted in Fig. 3. Note that $T_e(0)$ is much higher than T_s, as expected. $T_e(0)$ increases from 718 K to 1495 K with the increase of $\mathcal{F}$ from 10.6 μJ/cm^2 to 89.1 μJ/cm^2. Here, τ_{op} is set to be 2.7 ± 0.1 ps. The value of τ_{op} reasonably agrees with theoretical predictions ~2–4 ps for phonon temperatures in 500–900 K range.[27] The terms n_Γ^0 and n_K^0 are estimated by phonon distribution function with temperature at equilibrium of 10 K. The evolutions of T_e, n_K, and n_Γ as a function of the delay time at various $\mathcal{F}$ are shown in Figs. 5(a) and 5(b), respectively. The carrier temperature T_e rapidly decreases with increasing n_K and n_Γ within initial 2 ps, suggesting the cooling down of hot carriers via optical phonon emissions. After 2 ps, T_e gradually drops associated with the decrease of n_K and n_Γ.

It should be noted that our results reveal two distinct features in cooling dynamics: first, the feature of $T_e(0)$ versus $\mathcal{F}$ is intriguingly similar to that of τ_d versus $\mathcal{F}$, providing a direct indication of a strong correlation between T_e and τ_d. Second, the cooling rate of photoexcited carriers tends to drop at higher pump fluence as revealed in Fig. 3. The cooling dynamics in principle is governed by the number of photoexcited carriers (n, p) and the recombination rate $R_{\Gamma(K)}$. The relaxation time can then be expressed as $\tau_d = \min(n,p)/R_{\Gamma(K)}$.[12] $R_{\Gamma(K)}$ is mainly determined by carrier-phonon scattering and carrier distributions. As shown in Fig. 5(c), the photoexcited carriers (n, p) and the combined recombination rate $(R_{\Gamma(K)})$ increased with pump fluence at delay time of 1 ps. The increment of photoexcited carriers is about twice as fast as the recombination rate. Our calculations strongly suggest that $R_{\Gamma(K)}$ increases with the increase of n and p, but decreases with increasing T_e. In view of these results, we can readily see that τ_d increases with increasing T_e, qualitatively consistent with our findings displayed in Fig. 3. Finally, we try to address

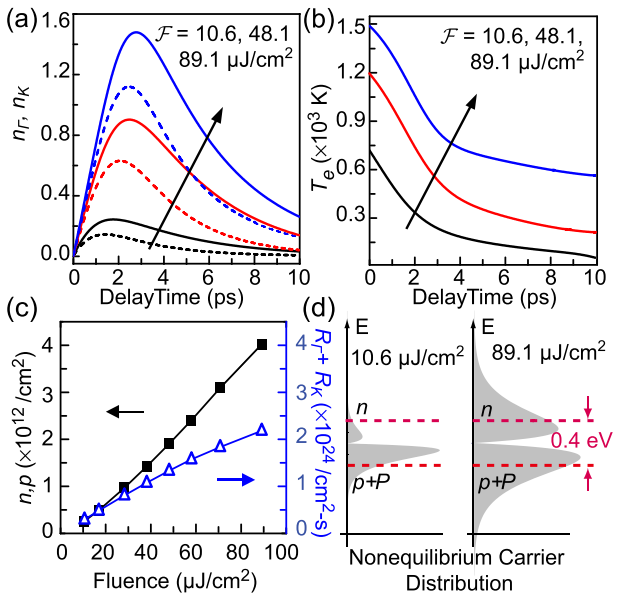

FIG. 5. (a) Phonon occupation numbers n_K (solid lines), n_Γ (dashed line) and (b) carrier temperature T_e as a function of probe delay time at different pump fluences. (c) The calculated photoexcited carriers and recombination rate at delay time of 1 ps as a function of pump fluence. (d) The initial photoexcited electron and hole distributions at pump fluences of 10.6 μJ/cm^2 and 89.1 μJ/cm^2, respectively.

why $R_{\Gamma(K)}$ reduces at high T_e. Figure 5(d) illustrates the calculated initial electron and hole distribution at low and high $\mathcal{F}$, respectively. Based on Eq. (3), the recombination rate $R_{\Gamma(K)}$ covers an energy window of those photoexcited electrons and holes within which the emission of optical phonons has an energy of $\hbar\omega_{\Gamma(K)}$. We roughly estimate the window to be about $\pm$ 0.2 eV indicated by dashed line in Fig. 5(d). It is clear that the energy distribution of most n and $p + P$ fairly falls within 0.4 eV at a low fluence. On the other hand, at a high fluence the tail of carrier distribution spreads out to higher energy states outside the window. Therefore, an increase of T_e with pump fluence can be attributed to a less efficient recombination rate at higher fluence.

The slowing down of the relaxation rate at high fluence is a direct consequence of the reduction of optical phonon emissions and the decrease of density of states near the charge neutral point. Recent theoretical and experimental studies reveal that electron-phonon interactions for optical phonon modes can be strongly layer-dependent,[28] and the substrate plays an important role in hot carrier cooling.[17] It reconciles the differences between our findings in CVD-grown monolayer graphene on quartz and those in epitaxial graphene or multilayer graphene on SiC substrate reported earlier.

V. CONCLUSIONS

In summary, using ultrafast optical-pump terahertz(THz)-probe spectroscopy, we have investigated the relaxation dynamics of photogenerated carriers in a chemical vapor deposited (CVD) graphene transferred on a quartz substrate. A few tens of femtoseconds after photoexcitation, we consider the hot carriers can be described by a Fermi-Dirac distribution function with carrier temperature and chemical potentials, resulting in a transient enhancement of the conductivity of graphene. We find that carrier relaxation time is insensitive to substrate temperature ranging from 10 K to 300 K, but sublinearly increases with increasing pump fluence. Our observations can be well interpreted by a recombination process involving electron-phonon scattering, and a set of rate equations to account for the temporal evolution of optical phonons. The relaxation time and photoexcited carrier temperature are found to be strongly correlated. Interband transition with emission of optical phonons plays a dominant role in cooling hot carriers. As a result of a broadening in carrier distribution induced by higher pump fluence, electron-phonon coupling becomes less efficient.

ACKNOWLEDGMENTS

We acknowledge Kou-Chien Hsu and Chien-Ming Tu for the fruitful discussions with the experiment. This project was supported by Department of Natural Science at National Science Council under Grant NSC 101-2628-M-007-002-MY3, Taiwan.

[1]A. H. Castro Neto, F. Guinea, N. M. Peres, K. S. Novoselov, and A. K. Geim, Rev. Mod. Phys. **81**, 109 (2009).
[2]V. Ryzhii, M. Ryzhii, and T. Otsuji, J. Appl. Phys. **101**, 024509 (2007).
[3]K. S. Novoselov, A. K. Geim, S. V. Morozov, D. Jiang, Y. Zhang, I. V. Grigorieva, and A. A. Firsov, Science **306**, 666 (2004).
[4]G. Liang, N. Neophytou, D. E. Nikonov, and M. S. Lundstrom, IEEE Trans. Electron Devices **54**, 677 (2007).
[5]J. R. Williams, L. DiCarlo, and C. M. Marcus, Science **317**, 638 (2007).
[6]V. Ryzhii, M. Ryzhii, and T. Otsuji, J. Appl. Phys. **101**, 083114 (2007).
[7]W. A. de Heer, C. Berger, X. Wu, P. N. First, E. H. Conrad, X. Li, T. Li, M. Sprinkle, J. Hass, M. L. Sadowski *et al.*, Solid State Commun. **143**, 92 (2007).
[8]K. V. Emtsev, A. Bostwick, K. Horn, J. Jobst, G. L. Kellogg, L. Ley, J. L. McChesney, T. Ohta, S. A. Reshanov, J. Röhrl *et al.*, Nature Mater. **8**, 203 (2009).
[9]J. Wintterlin and M. L. Bocquet, Surf. Sci. **603**, 1841 (2009).
[10]S. Bae, H. Kim, Y. Lee, X. Xu, J.-S. Park, Y. Zheng, J. Balakrishnan, T. Lei, H. R. Kim, Y. I. Song *et al.*, Nat. Nanotechnol. **5**, 574 (2010).
[11]T. Kampfrath, L. Perfetti, F. Schapper, C. Frischkorn, and M. Wolf, Phys. Rev. Lett. **95**, 187403 (2005).
[12]F. Rana, P. A. George, J. H. Strait, J. Dawlaty, S. Shivaraman, M. Chandrashekhar, and M. G. Spencer, Phys. Rev. B **79**, 115447 (2009).
[13]P. A. George, J. Strait, J. Dawlaty, S. Shivaraman, M. Chandrashekhar, F. Rana, and M. G. Spencer, Nano Lett. **8**, 4248 (2008).
[14]J. M. Dawlaty, S. Shivaraman, M. Chandrashekhar, F. Rana, and M. G. Spencer, Appl. Phys. Lett. **92**, 042116 (2008).
[15]H. Choi, F. Borondics, D. A. Siegel, S. Y. Zhou, M. C. Martin, A. Lanzara, and R. A. Kaindl, Appl. Phys. Lett. **94**, 172102 (2009).
[16]J. Strait, H. Wang, S. Shivaraman, V. Shields, M. Spencer, and F. Rana, Nano Lett. **11**, 4902 (2011).
[17]L. Huang, B. Gao, G. Hartland, M. Kelly, and H. Xing, Surf. Sci. **605**, 1657 (2011).
[18]H. Wang, J. H. Strait, P. A. George, S. Shivaraman, V. B. Shields, M. Chandrashekhar, J. Hwang, F. Rana, M. G. Spencer, C. S. Ruiz-Vargas *et al.*, Appl. Phys. Lett. **96**, 081917 (2010).
[19]C.-C. Tang, M.-Y. Li, L. J. Li, C. C. Chi, and J. C. Chen, Appl. Phys. Lett. **99**, 112107 (2011).
[20]A. C. Ferrari, J. C. Meyer, V. Scardaci, C. Casiraghi, M. Lazzeri, F. Mauri, S. Piscanec, D. Jiang, K. S. Novoselov, S. Roth *et al.*, Phys. Rev. Lett. **97**, 187401 (2006).
[21]Q. Wu and X. C. Zhang, Appl. Phys. Lett. **71**, 1285 (1997).
[22]J. M. Dawlaty, S. Shivaraman, J. Strait, P. George, M. Chandrashekhar, F. Rana, M. G. Spencer, D. Veksler, and Y. Chen, Appl. Phys. Lett. **93**, 131905 (2008).
[23]C. M. Randall and R. D. Rawcliffe, Appl. Opt. **6**, 1889 (1967).
[24]A. A. Falkovsky and L. A. Varlamov, Eur. Phys. J. B **56**, 281 (2007).
[25]Due to the fast intraband and interband carrier-carrier, including electron-hole, scattering time, we can reasonably assume the same carrier temperature for both electrons and holes as a quasi-equilibrium Fermi-Dirac distribution is reached.
[26]C. Park, F. Giustino, M. Cohen, and S. Louie, Nano Lett. **8**, 4229 (2008).
[27]N. Bonini, M. Lazzeri, N. Marzari, and F. Mauri, Phys. Rev. Lett. **99**, 176802 (2007).
[28]J.-A. Yan, W. Y. Ruan, and M. Y. Chou, Phys. Rev. B **79**, 115443 (2009).